Improvement of tube heat exchanger performance with perforated ring inserts, tube rotation and using nanofluids

Mohamed A. El-Magid Mohamed[1] · Andrés Meana-Fernández[2] · Antonio J. Gutiérrez-Trashorras[2]

Abstract

Many engineering applications, such as waste heat recovery, air-conditioning and refrigeration systems, include heat exchangers. In this work, the performance of a double-tube heat exchanger with a rotating tube, perforated ring inserts and nanofluids as working fluids has been studied. After developing a 3D numerical model, verifying its discretization and validating it with experimental results, an optimal design for maximizing heat transfer while keeping a relatively low pressure drop was found (11 eight-holed rings with a 2.2 pitch ratio). Increasing the cold fluid Reynolds number to 4946 and the inner tube rotational speed to 500 rpm increased the heat transfer coefficient from around 7500 to 9500 W $(m^2\ K)^{-1}$. Considering the nanofluids studied, the best performance was found with Cu nanoparticles, followed by Al_2O_3–Cu and Al_2O_3. With Cu nanoparticles at 3%, heat transfer coefficients above 12,100 W $(m^2\ K)^{-1}$ were obtained, increasing heat exchanger effectiveness from 27 to 51%. Pressure drop levels increased up to 235 Pa, resulting in increasing pumping requirements by around 0.1 kJ kg^{-1}. Hence, only very high flowrates would represent a problem when using the exchanger. Explanations for the underlying physical phenomena that cause the enhancement of heat transfer due to the rotational speed, the perforated rings and the nanofluids were provided. Turbulent kinetic energy contours, flow streamlines, and temperature contours were used to gain insight into the thermal and flow fields, identifying the mechanisms responsible for the enhancement of the heat exchanger effectiveness.

List of symbols

A_s	Heat transfer surface area (m^2)
C	Heat capacity rate (W K^{-1})
C_p	Specific heat capacity (J kg^{-1} K)
D_h	Hydraulic diameter of an annulus, $D_h = D_i - d_o$ (m)
D_i	Inner diameter of outer tube (m)
d_i	Inner diameter of inside tube (m)
d_o	Outer diameter of inside tube (m)
D_{ro}	Outer diameter of ring (m)
D_r	Diameter of hole in ring (m)
dr_i	Inner diameter of ring (m)
k	Thermal conductivity (W m^{-1} K)
L	Length of concentric tube (m)
$\dot{m}$	Mass flow rate (kg s^{-1})
NTU	Number of transfer units
N	Number of holes for rings
n	Number of rings
P	Pitch length (m)
PR	Pitch ratio (P/D_{ro})
Q	Heat transfer rate (W)
Re	Reynolds number
T	Temperature (K)
ΔT_{log}	Logarithmic mean temperature difference (K)
t	Thickness of rings (m)
U	Overall heat transfer coefficient (W m^{-2} K)
u	Axial flow velocity (m s^{-1})
Z	Direction coordinates along the tube

Greek symbols

ε	Effectiveness
ϕ	Solid volume fraction
ϕ_{Inc}	Viscous dissipation rate
μ	Dynamic viscosity (kg m^{-1} s)
ρ	Density (kg m^{-3})

Subscripts

avg	Average
cf	Cold fluid
hf	Hot fluid
i	Inlet

✉ Mohamed A. El-Magid Mohamed
  mabdelmagid@horus.edu.eg; m.abdelmagid@hotmail.com

1 Department of Mechanical Engineering, College of Engineering, Horus University, Damietta, Egypt

2 Department of Energy, University of Oviedo, Oviedo, Spain

max   Maximum
min   Minimum
nf   Nanofluid
o Outlet
s Nanoparticle
h Hybrid
f Fluid

Introduction

Improvements in heat exchanger thermal efficiency are crucial for achieving a better energy use and lower operational costs. Several methods to increase the efficiency of heat exchangers may be found in the literature and are classified into three groups: active, passive and combined. Active methods depend on an external power source to increase heat transfer (magnetic fields, mechanical systems, injections, or surface of fluid vibration). On the other hand, passive techniques enhance heat transfer by modifying the fluid flow or the heat exchanger geometry. The use of rougher surfaces, greater contact surfaces, fluid additives, coiled tubes, inserts or swirl flow devices are examples of passive methods. Combined methods take advantage of these two types, increasing heat transfer rate with a reduction pumping power.

Considerable research work has been done to investigate the flow and heat transfer characteristics in both passive and active methods. In 2000, Watel et al. [1] studied heat transfer in a rotating finned tube, reporting an increase in heat transfer when the tube was rotated with respect to the quiet tube. Four years after, Yakut and Sahin [2] studied conical ring inserts under forced convection, finding the best behavior with the smallest pitch arrangement. Nevertheless, Chen and Hsu [3] predicted that an increase in the fin spacing in an annular finned tube increased the average heat transfer coefficient. Experimental tests were performed by Kongkaitpaiboon et al. [4] to investigate heat transfer in a tube with circular ring inserts, finding heat transfer rate improvements of 57–195% with respect to a plan tube.

Concerning the use of nanofluids to improve heat transfer, the most recurrent ones are Al_2O_3, TiO_2 and CuO. In 2010, Duangthongsuk and Wongwises [5] experimentally verified an increase of 26% in the heat transfer coefficient when using TiO_2–water nanofluids instead of pure water. Yang et al. [6] investigated theoretically the forced convective heat transfer of Al_2O_3 and TiO_2–water nanofluids in a concentric annulus, finding a maximum Nusselt number at a particular nanoparticle volume fraction for Al_2O_3, but a continuous increase with concentration for TiO_2. Numerical simulations of Al_2O_3-water in a heated helically corrugate tube were performed by Darzi et al. [7], concluding that heat transfer increased with the nanoparticle volume fraction and the corrugation height and pitch. A Cu–TiO_2 hybrid nanofluid

was experimentally tested by Madhesh et al. [8] in a double-tube heat exchanger, finding an increase in the overall heat transfer coefficient of 68% at 1% concentration. The combined effect of twisted tape inserts and a TiO_2 nanofluid was studied by Ard and Kiatkittipong [9] using numerical simulations, observed a better performance in the counter-flow arrangement. Helical coil inserts combined with a TiO_2 nanofluid were investigated experimentally by Reddy and Rao [10], finding increases of around 14 and 11% in the heat transfer coefficient and the friction factor with 0.02% nanofluid concentration. In 2015, Chokphoemphun et al. [11] inserted winglet vortex generators in a tube heat exchanger, reporting better performances than with wire coils or twisted tapes. Ring-shaped ribs were studied by Huang et al. [12] and later by Singh et al. [13], who compared twisted tapes with solid rings, finding higher Nusselt numbers with the first ones. Perforated circular and conical rings were experimentally tested by Sheikholeslami et al. [14, 15], observing higher Nusselt numbers and lower friction factors with the increase in the number of holes. Other geometries, such as hexagonal conical ring inserts, were numerically studied by Sripattanapipat et al. [16], finding heat transfer rates 2.3–3.7 higher than for a plain tube. Polymeric nanofluids with twisted tapes were studied by Hazbehian et al. [17], reporting Nusselt values from 2.1 to 2.9 times greater than for a plain tube. Laminar convective heat transfer of a TiO_2 nanofluid moving through a uniformly heated tube were experimentally and numerically studied by Bajestan et al. [18], finding an increase in heat transfer coefficients with the increase in nanoparticle concentrations and Reynolds numbers. Cu and CuO-based nanofluids as well as carbon nanotubes have been also studied by Saeedan et al. [19] in a helically baffled heat exchanger with finned tubes, reporting better performances with the increase in nanofluid volume concentration.

The effect of rotating tubes in concentric tube exchangers using a Cu–water nanofluid was experimentally studied by El-Maghlany et al. [20], finding an enhancement of the heat exchanger effectiveness around 31%. This benefit was also observed by Ziyan et al. [21], who studied a rotating inner pipe with interrupted helical fins. Double and triple concentric tube heat exchangers were experimentally and numerically studied by Gomaa et al. [22], finding that the effectiveness of the triple tube exchanger was more than 50% higher. Nevertheless, the study of passive methods to improve heat transfer is still important when particular flow conditions are reached, as shown in the work of Forooghi et al. [23], who studied Reynolds number close to the transition region.

In 2017, Rao et al. [24] studied experimentally an Al_2O_3–water nanofluid at concentrations (0.1–0.4%), improving heat transfer rate by 2.5%. Kumar et al. [25] tested a Fe_3O_4 nanofluid, finding a 14.7% increase in the Nusselt number. Babu et al. [26] analyzed hybrid nanofluids,

presenting a summary of the recent research on synthesis, thermophysical properties, and heat transfer characteristics. Information about winglet vortex generators may be found in [27, 28]. In this sense, conical strips were found by Liu et al. [29] to multiply Nusselt numbers by more than 7.5 times under laminar flow, while mesh rings were able to increase them by around 3.5 times [30]. The effect of the eccentricity of tube rotation in the heat transfer increase was studied by Ali et al. [31]. The performance of Cu- and Al_2O_3–water was compared by Siadaty and Kazazi [32], finding that Cu-based nanofluids outperformed Al_2O_3 ones. Muszynski and Andrzejczyk [33] combined heat exchanger surface modification with microjet impingement in a proposal of a heat exchanger prototype. Corrugated rings were simulated by Al-Obaidi [34], increasing heat transfer by more than 2.6 times, while values from 1.6 to 2.8 times were reported by Nakhchi and Esfahani [35] for perforated conical rings with a Cu-water nanofluid. Similar studies may be found in [36–38], reporting enhancements from 3.3 to 7.6 times in Nusselt numbers. Comparing longitudinal and annular fins, the numerical simulations of Nada and Said [39] under free convection heat transfer showed a better performance of the longitudinal ones. Yadav and Sahu [40] studied helical surface disk turbulators, finding increases of around 3.3 times in Nusselt numbers.

More recent research confirms the benefits of nanofluids for enhancing heat transfer, with Qi et al. [41] reporting increases of heat transfer rates by up to around 15% using TiO_2–water. Enhancements of 16.3% were found with graphene nanofluids in rotating coaxial tubes with double twisted tapes [42]. In 2020, Bezaatpour and Goharkhah [43] studied the addition of an external magnetic field, hinting at improvements of heat transfer by up to 3.2 times, while Thejaraju et al. [44] reported experimental values of Nusselt numbers up to 4 times higher when using a para-winglet tape. The neural network model developed by Bahiraei et al. [45] also predicts an improvement when using graphene nanoplatelets in a rotating tube with twisted tapes. However, numerical models for flow simulation continue to be the standard, as shown in [46], who studied a Fe_3O_4 nanofluid combined with longitudinal strip inserts and trapezoidal twisted tape inserts. Tapered wire coils combined with an Al_2O_3–MgO nanofluid showed an increase of 47% in Nusselt numbers in the work of Singh and Sarkar [47]. Vented cavities combined with Al_2O_3–Cu [48] and Cu [49] nanofluids and the rotation of a tube have been also reported to improve heat transfer. When rotating tubes with twisted tapes and alternating rotational axes containing two-phase nanofluids, Singh et al. [50] also found increases up to 10% in Nusselt numbers.

Finally, the effect of tube rotation has shown to be beneficial for the faster melting of phase-change materials when dealing with thermal energy storage in the experiments reported by Fathi and Mussa [51]. In addition, dynamic viscosity was found to be a key parameter by Heydari et al. [52], who used statistical models to analyze the behavior of a hybrid nanofluid composed of multi-walled carbon nanotube and Al_2O_3, confirming experimentally that optimal heat exchanger performance was reached when all nanofluids could flow. The optimum nanofluid composition is relevant for applications where the selection of the working fluid has a significant impact in the heat transfer performance [53–55].

As a summary, Table 1 collects the main studies selected from the literature, classifying them depending on the heat exchanger morphology and nanofluid employed.

According to the existing bibliography, the combination of active and passive methods for heat transfer enhancement in heat exchangers is of interest, with many combinations still lacking a deep study. In addition, the role of nanofluids seems of vital importance to further enhance the performance of the heat exchanger, with the addition of tube rotation contributing to a better mixing and heat transfer. In the present work, the aim is the study of the performance of a tube heat exchanger combining the effects of a rotating tube and perforated ring inserts when Al_2O_3, Cu and hybrid Al_2O_3–Cu nanofluids are used as working fluids. The importance of the studied geometry relies on the increase in the heat transfer surface area, allowing to reduce the size of the heat exchanger. Furthermore, the presence of circular rings is supposed to increase turbulence levels, mixing and heat convection coefficients. Moreover, the use of nanofluids is bound to increase heat transfer, whereas the rotation of the inner tube is supposed to achieve a better fluid mixing. Consequently, many engineering applications, such as waste heat recovery processes, air-conditioning and refrigeration systems, would be benefited from including the studied geometry in heat exchangers.

Physical model description

Geometry

A three-dimensional model of a double-tube heat exchanger has been developed, consisting of an inner tube with perforated circular ring (PCR) inserts enclosed by an outer tube, as depicted in Fig. 1. The hot working fluid, water, circulates through the inner tube, whereas the cold working fluid, water or nanofluid, flows through the outer annulus in a counterflow arrangement, as shown in Fig. 1a. The heat exchanger length is 1200 mm. The diameters of the inner (d_i) and outer tubes (D_i) are 25.4 and 76.2 mm, respectively, both with a thickness of 2 mm. The inner tube is made of high thermal conductive copper, while the outer tube is made of Plexiglass. Rings are made of copper, with a thickness t of

Table 1 Summary of main of main studies selected from the literature

Author	Heat exchanger morphology	Type of study	Working fluid	Main results
Chen and Hsu [3]	Annular finned tube	Experimental	Air	Average heat transfer coefficient increases with fin spacing
Kongkaitpaiboon et al. [4]	Circular rings	Experimental	Air	Heat transfer enhanced by 57–195%
Yang et al. [6]	Concentric annulus	Numerical	Al_2O_3, TiO_2	Optimum nanoparticle volume fraction for increasing Nusselt number
Singh et al. [13]	Twisted tapes, rings	Experimental	Air	Nusselt number of rings: 107 Nusselt number of twisted tapes: 293
Sheikholeslami et al. [14]	Perforated circular ring	Experimental	Air	Nusselt number increases, and friction factor decreases with number of holes
Sripattanapipat et al. [16]	Hexagonal conical ring	Numerical	Cu	Heat transfer enhanced by 2.3–3.7 times
Saeedan et al. [19]	Double pipe helically baffled	Numerical	Cu, CuO, C nanotube	Heat transfer coefficient and pressure gradient increased
El-Maghlany et al. [20]	Rotating inner tube	Experimental	Cu	NTU increased by 51.4% and exchanger effectiveness by 30.7%
Ziyan et al. [21]	Rotating inner pipe with helical fins	Experimental	Air	Nusselt number enhanced about 7.5 times
Nakhchi and Esfahani [35]	Perforated conical ring	Numerical	Cu	Nusselt number enhanced by 278.2%
Nada and Said [39]	Annular and longitudinal rectangular fins	Numerical	Air	Heat transfer rate increased by 78.6%
Yadav and Sahu [40]	Helical surface disk turbulators	Experimental	Water/Air	Nusselt number increased by 3.28 times
Bahiraei et al. [42]	Rotating coaxial tube with double twisted tapes	Numerical	Graphene	Heat transfer coefficient increased by 16.3% at a 2.5 twist ratio
Thejaraju et al. [44]	Novel para-winglet tape	Experimental	Air	Nusselt number was enhanced by 407%
Bahiraei et al. [45]	Rotating coaxial tube with double twisted tapes	Numerical	Graphene	Rotation of the tube improved heat transfer coefficient and increased pressure drop
Murali et al. [46]	Trapezoidal twisted tape	Numerical	Fe_3O_4	Heat transfer rate increased by 78.6%
Singh and Sarkar [47]	Tapered wire coils in double tube	Experimental	Al_2O_3–MgO	Nusselt numbers increased by 84%
Jasim et al. [48]	Inner rotating cylinder	Numerical	Al_2O_3-Cu	Heat transfer enhanced up to 10.6%
Moayedi [49]	Double rotating cylinders in vented cavity	Experimental	Cu	Nusselt number enhanced by 331.95%

2 mm. Their inner diameter dr_i is 25.4 mm, while three different outer diameters Dr_o of 35.4, 45.4 and 55.4 mm have been tested. Several ring holes N (0, 4, 8) with a diameter D_r of 6 mm have been made to the rings. The simulated pitch length P values, representing the distance between the center of two consecutive rings, are 100 and 200 mm. Two sets of simulations with a number of rings $n = 5$ and $n = 11$ have been performed. Hence, the pitch ratio PR values, defined as the ratio between the pitch length and the outer diameter of ring, become 2.82, 2.2 and 1.8 when $n = 11$ and 5.64, 4.4 and 3.61 when $n = 5$. Figure 1b shows a scheme of the geometry with all the key parameters defining each simulated case. Finally, the inner tube has been rotated at different speeds, from 0 to 500 rpm, whereas four different working cold fluids have been simulated: water, Al_2O_3–water and Cu–water nanofluids, and a hybrid Al_2O_3–Cu–water nanofluid.

Mesh generation and boundary conditions

The mesh was generated in ANSYS Fluent®, using a combination of hexahedral and tetrahedral cells, as shown in Fig. 2. Figure 3 represents the boundary conditions applied to the simulation domain. The fluid inlets are defined as velocity-inlet boundary conditions, whereas the outlets are defined as pressure-outlet boundary conditions. Velocities are calculated so that the Reynolds number of the cold fluid Re_{cf}, entering through the annulus at a temperature of 301 K, ranges between 2473 and 4947. Therefore, the different fluid properties depending on the nanofluid volume concentration ϕ values simulated, 1, 2 and 3%, have been considered. The Reynolds number of the hot water, entering the inner tube at a temperature of 333 K, has been fixed at 9780. The no-slip wall condition is applied to the tubes and rings, considering

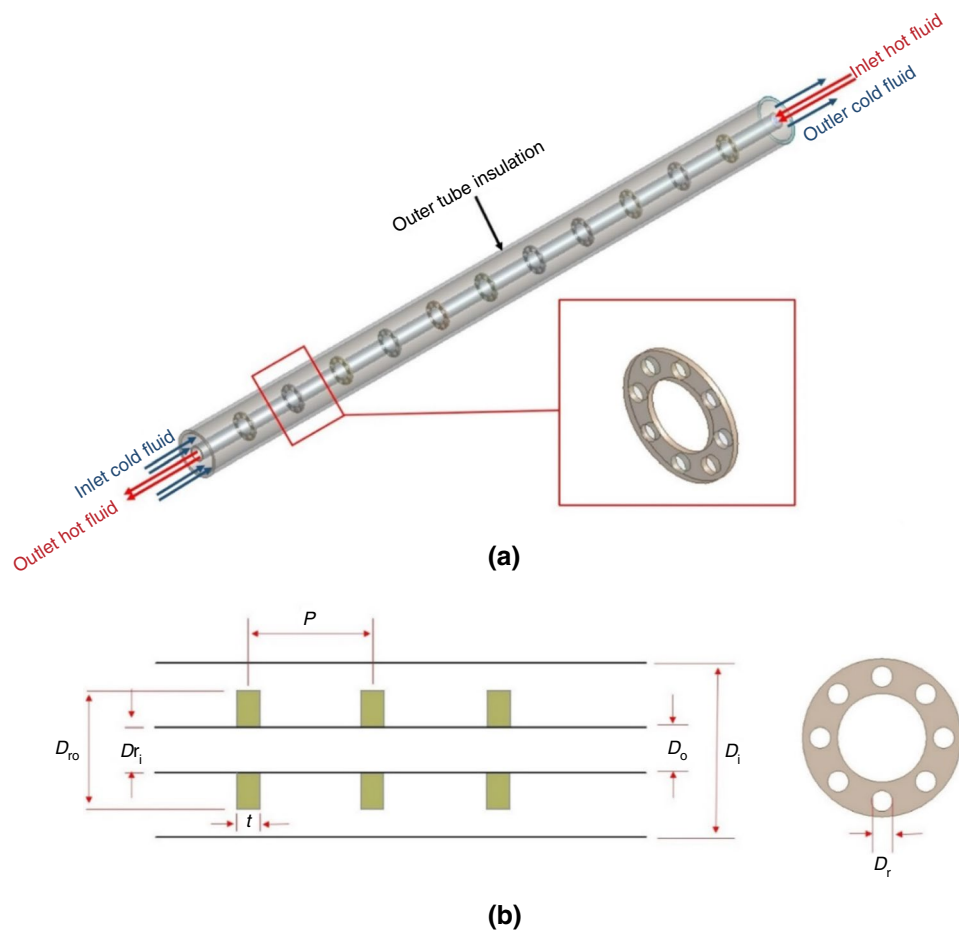**Fig. 1 a** Geometry of the heat exchanger, **b** geometrical parameters of the tubes and rings

(a)

(b)

Fig. 2 a Double-tube heat exchanger mesh, **b** detail of the mesh with perforated circular ring inserts
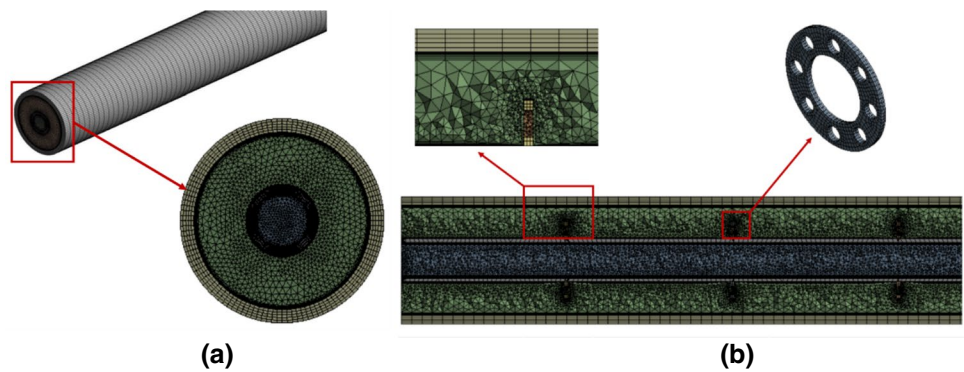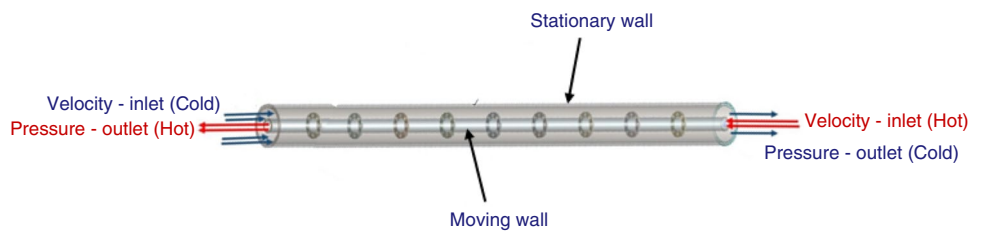

(a)   (b)

Fig. 3 Boundary conditions applied to the domain

that the outer tube is an insulated fixed wall and the inner tube with rings is rotated at speeds from 0 to 500 rpm in increments of 100 rpm.

Governing equations and numerical solver

Forced convection equations were used to describe the flow in the domain, assuming incompressible, steady-state and homogeneous flow. The finite volume method was used to discretize and solve continuity, momentum and energy equations, using ANSYS Fluent® software:

- Continuity equation:

$$\frac{1}{r}\frac{\partial (ru_r)}{\partial r} + \frac{1}{r}\frac{\partial u_\theta}{\partial \theta} + \frac{\partial u_z}{\partial z} = 0 \qquad (1)$$

- Momentum equation for radial component r:

$$\rho\left(u_r\frac{\partial u_r}{\partial r} + \frac{u_\theta}{r}\frac{\partial u_r}{\partial \theta} + u_z\frac{\partial u_r}{\partial z} - \frac{u_\theta^2}{r}\right)$$
$$= \rho g_r - \frac{\partial \rho}{\partial r} + \mu\left[\frac{1}{r}\frac{\partial}{\partial r}r\left(\frac{\partial u_r}{\partial r}\right) + \frac{1}{r^2}\frac{\partial^2 u_r}{\partial \theta^2}\right. \qquad (2)$$
$$\left. + \frac{\partial^2 u_r}{\partial z^2} - \frac{2}{r^2}\frac{\partial u_\theta}{\partial \theta} - \frac{u_r}{r^2}\right]$$

- Momentum equation for tangential component θ:

$$\rho\left(u_r\frac{\partial u_\theta}{\partial r} + \frac{u_\theta}{r}\frac{\partial u_\theta}{\partial \theta} + u_z\frac{\partial u_\theta}{\partial z} - \frac{u_r u_\theta}{r}\right)$$
$$= \rho g_\theta - \frac{1}{r}\frac{\partial \rho}{\partial \theta} + \mu\left[\frac{1}{r}\frac{\partial}{\partial r}r\left(\frac{\partial u_\theta}{\partial r}\right) + \frac{1}{r^2}\frac{\partial^2 u_\theta}{\partial \theta^2}\right. \qquad (3)$$
$$\left. + \frac{\partial^2 u_\theta}{\partial z^2} - \frac{2}{r^2}\frac{\partial u_r}{\partial \theta} - \frac{u_\theta}{r^2}\right]$$

- Momentum equation for axial component z:

$$\rho\left(u_r\frac{\partial u_z}{\partial r} + \frac{u_\theta}{r}\frac{\partial u_z}{\partial \theta} + u_z\frac{\partial u_z}{\partial z}\right)$$
$$= \rho g_z - \frac{\partial \rho}{\partial r} + \mu\left[\frac{1}{r}\frac{\partial}{\partial r}r\left(\frac{\partial u_z}{\partial r}\right)\right. \qquad (4)$$
$$\left. + \frac{1}{r^2}\frac{\partial^2 u_z}{\partial \theta^2} + \frac{\partial^2 u_z}{\partial z^2}\right]$$

- Energy equation:

$$\left(u_r\frac{\partial T}{\partial r} + \frac{u_\theta}{r}\frac{\partial T}{\partial \theta} + u_z\frac{\partial T}{\partial z}\right)$$
$$= \frac{\dot{q}g}{C_p} + \alpha\left[\frac{1}{r}\frac{\partial}{\partial r}r\left(\frac{\partial T}{\partial r}\right)\right. \qquad (5)$$
$$\left. + \frac{1}{r^2}\frac{\partial^2 T}{\partial \theta^2} + \frac{\partial^2 T}{\partial z^2}\right] + \frac{\phi_{Inc}}{\rho C_p}$$

where the viscous dissipation rate is

$$\phi_{Inc} = 2\mu\left[\left(\frac{\partial u_r}{\partial r}\right)^2 + \left(\frac{1}{r}\frac{\partial u_\theta}{\partial \theta} + \frac{u_r}{r}\right)^2 + \left(\frac{\partial u_z}{\partial z}\right)^2\right]$$
$$+ \mu\left[\left(\frac{1}{r}\frac{\partial u_r}{\partial \theta} + \frac{\partial u_\theta}{\partial r} - \frac{u_\theta}{r}\right)^2 + \left(\frac{1}{r}\frac{\partial u_z}{\partial \theta} + \frac{\partial u_\theta}{\partial z}\right)^2\right.$$
$$\left. + \left(\frac{\partial u_z}{\partial r} + \frac{\partial u_r}{\partial z}\right)^2\right]$$
$$\qquad (6)$$

The RNG k-ε model with enhanced wall treatment was selected for the closure of turbulence to solve the Reynolds-averaged Navier–Stokes (RANS) equations. This model has shown to be more accurate than the standard k-ε in the literature [9, 22], as it accounts for the effects of the smaller scales of motion by changing the term of turbulence production in the transport equations. In addition, it has been found suitable for low Reynolds numbers and swirling flow [22], achieving a higher accuracy in rotating and recirculating flows such as the ones present in this work.

A second-order upwind scheme has been used for the discretization of the domain, while the SIMPLE algorithm has been selected for the coupling of pressure and velocity fields. Convergence criteria were set to 10^{-5} for the continuity and momentum equations, and to 10^{-6} for the energy equation. A flowchart summarizing the methodology used in this work is added in Fig. 4.

Thermophysical properties of fluids

Based on the approach adopted in the works of Sripattanapipat et al. [19] and Singh and Sarkar [42], the single-phase model was selected to model the nanofluids, with the assumptions that nanoparticles and the base fluid are in thermal equilibrium, and they flow as a single-phase suspension. This allowed to decrease computational time while keeping a reasonable accuracy, according to the literature. Nanofluids have been modeled as incompressible fluids with constant physical properties, evaluated with specific correlations obtained from the literature. Table 2 collects the properties of pure water and the nanoparticles that have been introduced to generate the nanofluids.
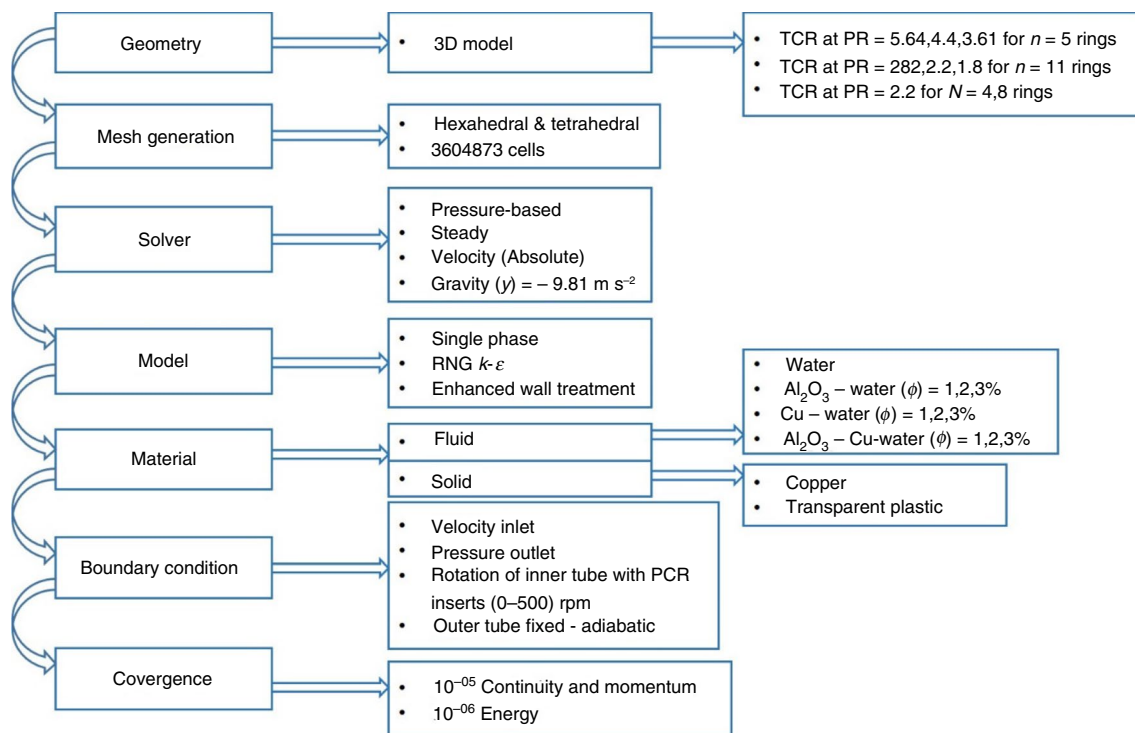
Fig. 4 Methodology followed in this work

Table 2 Thermophysical properties of pure water and nanoparticles

Physical properties	ρ/kg m^{-3}	C_p/J kg^{-1} K^{-1}	k/W m^{-1} K^{-1}
Pure water [20]	997.1	4179	0.6
Al$_2$O$_3$ [32]	3970	765	36
Cu [20]	8933	385	385

Hence, the effective density of the nanofluid ρ_{nf} is given by Eq. 7 [20]:

$$\rho_{nf} = (1 - \phi)\rho_f + \phi\rho_s \tag{7}$$

where ρ_f is the density of water, ρ_s is the density of nanoparticles, and ϕ is the solid volume fraction. The volumetric heat capacity of the nanofluid $\left(\rho C_p\right)_{nf}$ is obtained from Eq. 8 [20]:

$$\left(\rho C_p\right)_{nf} = (1 - \phi)\left(\rho C_p\right)_f + \phi\left(\rho C_p\right)_s \tag{8}$$

where $\left(\rho C_p\right)_f$ and $\left(\rho C_p\right)_s$ are the volumetric heat capacities of water and the nanoparticles, respectively. The effective thermal conductivity of the nanofluid k_{nf} is given by Eq. 9 [10]:

$$k_{nf} = k_f\left[\frac{k_s + 2k_f + 2\phi(k_s - k_f)}{k_s + 2k_f - \phi(k_s - k_f)}\right] \tag{9}$$

where k_f and k_s are thermal conductivities of water and the nanoparticles. Finally, the effective dynamic viscosity of the nanofluid μ_{nf} is obtained from Eq. 10 when $\phi \leq 5\%$

$$\mu_{nf} = (1 + 2.5\phi)\mu_f \tag{10}$$

where μ_f is dynamic viscosity of the fluid (water).

For hybrid nanofluids, the effective density for a mixture of two nanoparticle types ρ_{hnf} may be estimated from Eq. 11 [26]:

$$\rho_{hnf} = \phi_{s1}\rho_{s1} + \phi_{s2}\rho_{s2} + \left(1 - \phi_h\right)\rho_f \tag{11}$$

where ρ_f is density of water, and ρ_{s1} and ρ_{s2} are the densities of the two nanoparticle types. The volume concentration ϕ_h is calculated from Eq. 12 [26]:

$$\phi_h = \phi_{s1} + \phi_{s2} \tag{12}$$

where ϕ_{s1} and ϕ_{s2} are the solid volume fractions of the two types of nanoparticles. Consequently, the effective heat capacity of a hybrid nanofluid may be obtained from Eq. 13 [26]:

$$\left(\rho C_p\right)_{hnf} = \phi_{s1}\rho_{s1}C_{p,s1} + \phi_{s2}\rho_{s2}C_{p,s2} + \left(1 - \phi_h\right)\rho_f C_{p,f} \tag{13}$$

where $C_{p,s1}$ and $C_{p,s2}$ are the specific heats of the two nanoparticle types. The effective dynamic viscosity of hybrid nanofluids may be obtained from Eq. 14 [26]:

$$\mu_{hnf} = \left(1 + 2.5\phi_h + 6.2\phi_h^2\right)\mu_f \tag{14}$$

And the effective thermal conductivity may be estimated with the modified Maxwell model as shown in Eq. 15 [26]:

$$k_{hnf} = k_f \left[\frac{\frac{\phi_{s1}k_{s1}+\phi_{s2}k_{s2}}{\phi_{hnf}} + 2k_f + 2\left(\phi_{s1}k_{s1} + \phi_{s2}k_{s2}\right) - 2\phi_{hnf}k_f}{\frac{\phi_{s1}k_{s1}+\phi_{s2}k_{s2}}{\phi_{hnf}} + 2k_f - \left(\phi_{s1}k_{s1} + \phi_{s2}k_{s2}\right) + \phi_{hnf}k_f} \right] \tag{15}$$

with k_{s1} and k_{s2} being the thermal conductivities of the two nanoparticle types.

Grid independence study

A grid independence study was conducted to verify the numerical accuracy of the model, using the exchanger without rings and rotation of the inner tube, and water at a Reynolds number $Re_{cf} = 2470$ as working cold fluid. The number of transfer units NTU and the pressure drop were monitored as convergence variables As shown in Fig. 5, the grid with 3,604,873 cells and discretization error around 0.98% for the NTU was considered accurate enough for the purpose of this study.

Experimental validation

The results of NTU and pressure drop from the selected mesh were compared with the results from El-Maghlany et al. [20] for water and the Cu–water nanofluid at 3% volume concentration. The numerical results agree consistently with the experimental results, as shown in Fig. 6, with the maximum deviation for NTU being 4.3% and 4.88% for water and Cu-water nanofluid, respectively, and 4% and 3.62% for the pressure drop. Hence, it can be concluded that the model is valid for the purpose of this study. As the results from the model matched the experimental results with reasonable accuracy, it was decided to keep using the RNG k-ε model throughout the rest of the work.

Numerical data processing

The results from the simulations were processed to obtain the global variables that describe the heat exchanger performance. Firstly, the heat lost from the hot fluid was obtained as:

$$Q_{hf} = \dot{m}_{hf}C_{p,hf}\left(T_{hf,i} - T_{hf,o}\right) \tag{16}$$

where $\dot{m}_{hf}$ is the hot fluid (water) mass flow rate, $C_{p,hf}$ is its specific heat, and $(T_{hf,i} - T_{hf,o})$ is its temperature difference between inlet and outlet.
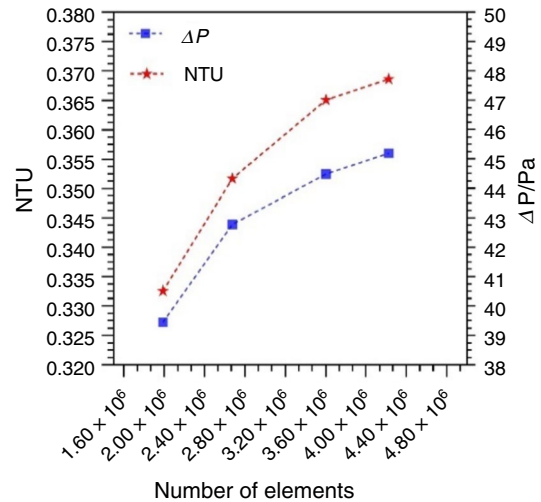

Fig. 5 Grid independence study at $Re_{cf} = 2470$

Similarly, the heat absorbed by the cold fluid was obtained as:

$$Q_{cf} = \dot{m}_{cf}C_{p,cf}\left(T_{cf,o} - T_{cf,i}\right) \tag{17}$$

where $\dot{m}_{cf}$ is the cold fluid (nanofluid) mass flow rate, $C_{p,cf}$ is its specific heat, and $(T_{cf,o} - T_{cf,i})$ is its temperature difference of between outlet and inlet.

Allowing to calculate the average heat transfer rate as the mean of both values:

$$Q_{avg} = \frac{Q_{hf} + Q_{cf}}{2} \tag{18}$$

Leading to the obtention of the overall heat transfer coefficient:

$$U = \frac{Q_{avg}}{A_s\Delta T_{LM}} \tag{19}$$

where A_s is the heat transfer surface area and ΔT_{LM} is the logarithmic mean temperature difference, obtained as:

$$\Delta T_{LM} = \frac{\left(T_{hf,o} - T_{cf,i}\right) - \left(T_{hf,i} - T_{cf,o}\right)}{\ln \frac{T_{hf,o}-T_{cf,i}}{T_{hf,i}-T_{cf,o}}} \tag{20}$$
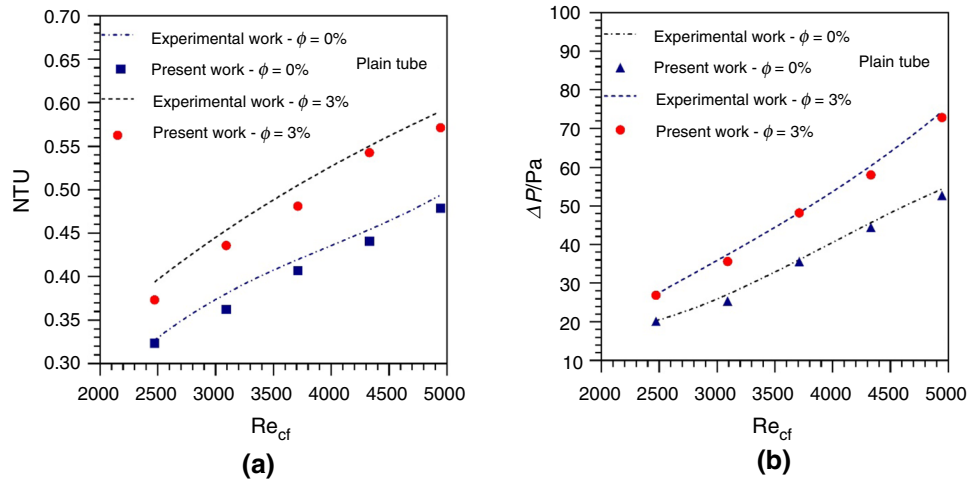
Then, defining C_{min} and C_{max} as the minimum and maximum heat fluid capacity rates:

$$C_{min} = \min\left(C_h, C_c\right), C_{max} = \max\left(C_h, C_c\right),$$
$$C_h = \dot{m}_{hf}C_{p,hf}, C_c = \dot{m}_{cf}C_{p,cf} \tag{21}$$

It is possible to obtain the number of transfer units (NTU) as:

Fig. 6 Experimental validation: **a** NTU, **b** Pressure drop

(a)

(b)

$$\text{NTU} = \frac{UA_s}{C_{\min}} = \frac{Q_{\text{avg}}}{\Delta T_{\log} C_{\min}} \tag{22}$$

and the effectiveness of the heat exchanger as:

$$\left(\varepsilon = \frac{1 - \exp\left[\left(-\text{NTU}\left(1 - \frac{C_{\min}}{C_{\max}} \right) \right) \right]}{1 - \frac{C_{\min}}{C_{\max}} \exp\left[\left(-\text{NTU}\left(1 - \frac{C_{\min}}{C_{\max}} \right) \right) \right]} \right) \tag{23}$$

The overall heat transfer coefficient of the heat exchanger may be obtained as:

$$h = \frac{Q_{\text{avg}}}{A_s \left(T_w - T_b \right)} \tag{24}$$

where T_w is the wall temperature and T_b is the bulk mean fluid temperature. Finally, the required pumping power for the heat exchanger is calculated as [42]:

$$W = \left(\dot{V}\Delta P \right)_{\text{cf}} + \left(\dot{V}\Delta P \right)_{\text{hf}} \tag{25}$$

where ΔP (Pa) is the pressure drop, and $\dot{V}$ is the volumetric flow rate ($\text{m}^3 \text{ s}^{-1}$).

Results and discussion

Firstly, the effect of varying the pitch ratio and the number of perforated holes in the ring inserts will be assessed using water as the cold fluid and without rotation of the inner tube. After selecting the most suitable geometrical configuration, the performance of the exchanger will be assessed by varying the nanofluid and the rotational speed of the inner tube, evaluating the heat transfer characteristics and the flow field behavior.

Effect of geometric parameters

Effect of pitch ratio (PR)

Figure 7 shows the effect of varying the pitch ratio and the cold fluid Reynolds number when $n = 5$ solid rings are added to the inner tube, resulting in a pitch length $P = 200$ mm. The three values of the outer ring diameter tested lead to three pitch ratio values: 5.64, 4.4 and 3.61. Looking at Fig. 7a, which shows these effects on the heat transfer coefficient, it may be appreciated that the increase in the Reynolds number leads to an increase in the heat transfer coefficient. The increase in the flow speed and turbulence may contribute to a better mixing of the fluid adjacent to the tube, increasing thus the heat flux across the tube walls. For instance, at the maximum Reynolds number tested, 4946, the heat transfer coefficient increases around 45% with respect to the lowest one, 2473. The circular ring inserts seem to increase turbulence while also providing additional heat transfer surface, enhancing transfer coefficients by 4.93, 8.33 and 9.35% as the pitch ratio decreases due to the increase in the ring diameter. Nevertheless, the insertion of rings results in an increase in the pressure drop, as shown in Fig. 7b. At the maximum Reynolds number, the pressure drop increases as the ring diameter increases and the pitch ratio decreases: 28, 85 and 670% higher values are found as PR passes from 5.64 to 4.4 and 3.61. As the difference between the heat transfer coefficients reached with PR = 4.4 and 3.61 is 0.95%, it may be concluded that increasing the ring diameter resulting in PR values below 4.4 does not enhance substantially heat transfer, while it increases extremely the pressure drop.

For the second set of simulations with $n = 11$ solid rings, the pitch length P becomes 100 mm and the pitch ratio PR values turn into 2.82, 2.2 and 1.8. Looking at the results depicted in Fig. 8a, trends similar to the ones in Fig. 7 are visible, with the heat transfer coefficient increasing with the Reynolds number and with the decrease in the pitch ratio.

Fig. 7 Effect of pitch ratio at $n = 5$ and $N = 0$; **a** heat transfer coefficient, **b** pressure drop

(a)

(b)
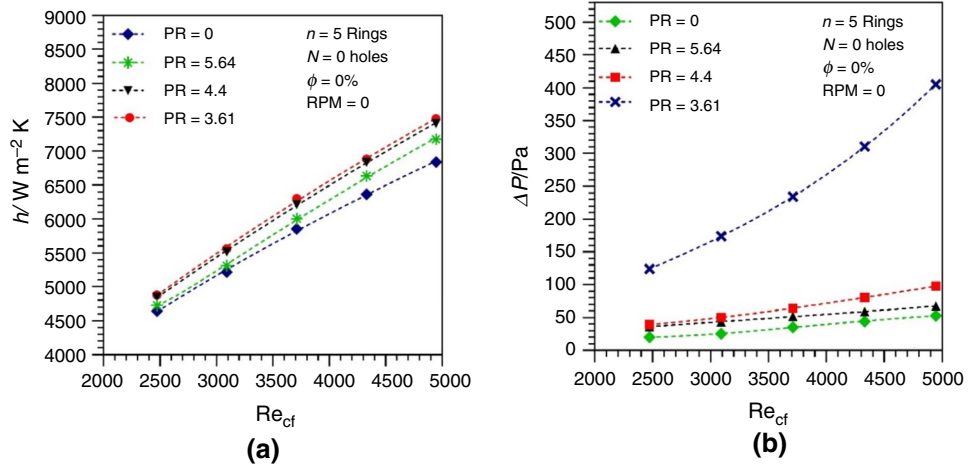
Nevertheless, comparing the results with the ones for $n = 5$ (Fig. 7), it may be appreciated that higher heat transfer coefficients are reached when a larger number of rings are inserted on the tube, passing from a maximum of around 7400–7800 W $(m^2 K)^{-1}$. At the highest Reynolds number, 4946, as the pitch ratio decreases from 2.82 and 2.2 to 1.8, the heat transfer coefficient increases by 7.54, 9.73 and 14.3% with respect to the case without rings. Nevertheless, at PR = 1.8, the pressure drop, as shown in Fig. 8b, becomes too large (838.8% with respect to the case without rings) in comparison with the beneficial effect in the heat transfer coefficient. A PR = 2.2 is able to increase the heat transfer coefficient substantially with just an increase of 168.72% in the pressure drop.

After analyzing the results regarding the pitch ratio and the number of rings, the following results are presented with the optimal configuration that achieves a high heat transfer without a great penalty in the pressure drop: $n = 11$ rings with a pitch ratio PR = 2.2.

Effect of the number of ring holes *N*

When perforated circular rings with $N = 4$ and 8 holes were inserted on the heat exchanger inner tube with the configuration selected in the previous subsection ($n = 11$, PR = 2.2), the results shown in Fig. 9 were obtained. The holes contribute to reaching higher heat transfer coefficients than with solid rings, as it may be appreciated in Fig. 9a, and, at the same time, reduce the pressure drop across the exchanger caused by the presence of the rings, as it is visible in Fig. 9b. With 4 and 8 holes, the heat transfer coefficient increases by 0.78 and 4.64%, respectively, at the maximum Reynolds number of 4946, while the pressure drop decreases by 6.53 and 16.67%.

The mechanism related to the pressure drop decrease, as well as the heat transfer enhancement, may be appreciated in Fig. 10, which depicts velocity vectors in a longitudinal plane of the heat exchanger tubes. Comparing the image at the top, corresponding to solid rings, with the bottom one, corresponding to $N = 8$ holes, it may be observed that velocity vectors become of greater magnitude near the ring holes,

Fig. 8 Effect of pitch ratio at $n = 11$ and $N = 0$; **a** heat transfer coefficient (*h*), **b** pressure drop
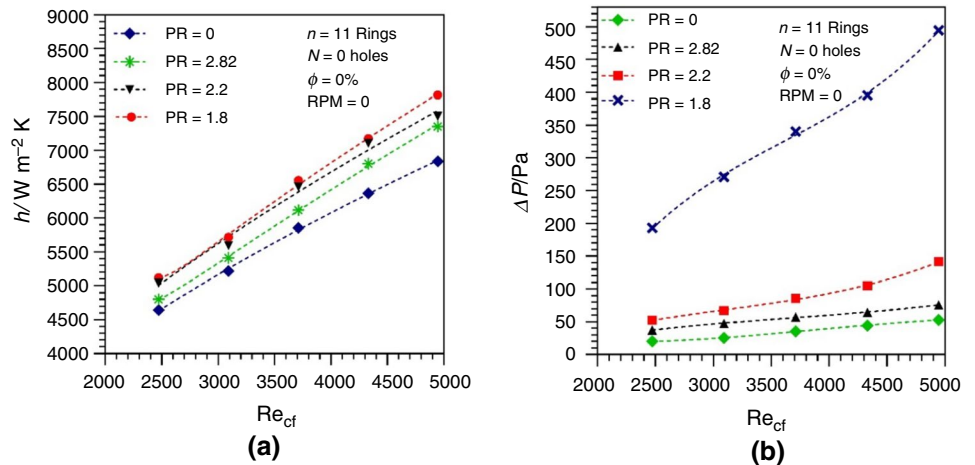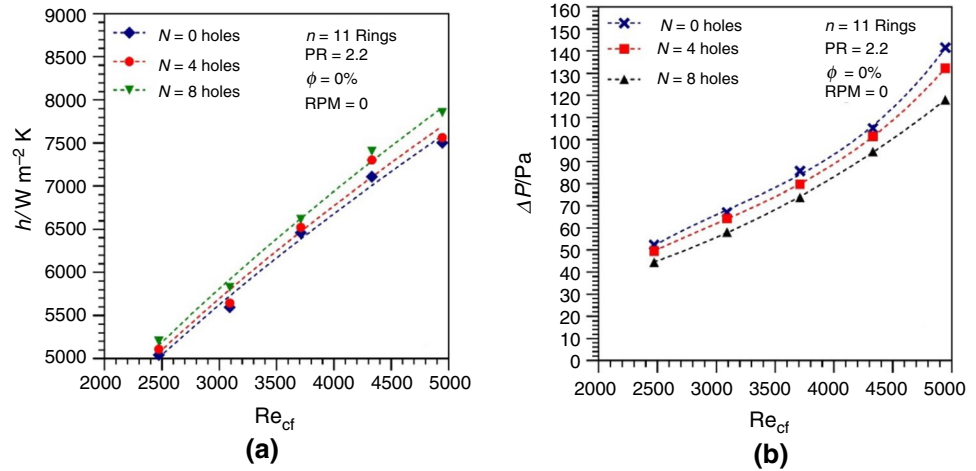

(a)

(b)

Fig. 9 Effect of number of holes; **a** heat transfer coefficient, **b** pressure drop

showing also changes in direction. These modifications in the velocity vectors near the holes may be related to the disruption of the thermal boundary layer and the generation of strong recirculating flows, allowing for a higher turbulent mixing and increasing heat transfer rates, as well as posing less resistance to axial flow and thus reducing the pressure drop.

Effect of inner tube rotation and nanofluid type and concentration

Following the previous results, the heat exchanger configuration with $n = 11$ rings with $N = 8$ holes placed on the inner tube with a pitch ratio PR = 2.2 was selected for subsequent

analyses, being the one that maximized heat transfer while reducing the pressure drop as much as possible. After fixing the heat exchanger geometry, the effects of inner tube rotation, nanofluid type and concentration are presented in this subsection.

Heat transfer coefficient

Figure 11 shows the heat transfer coefficient values for different tube rotational speeds as a function of the Reynolds number and the nanoparticle concentration for water and three different nanofluids based on Al_2O_3, Cu, and hybrid Al_2O_3–Cu nanoparticles. Apart from the increase observed
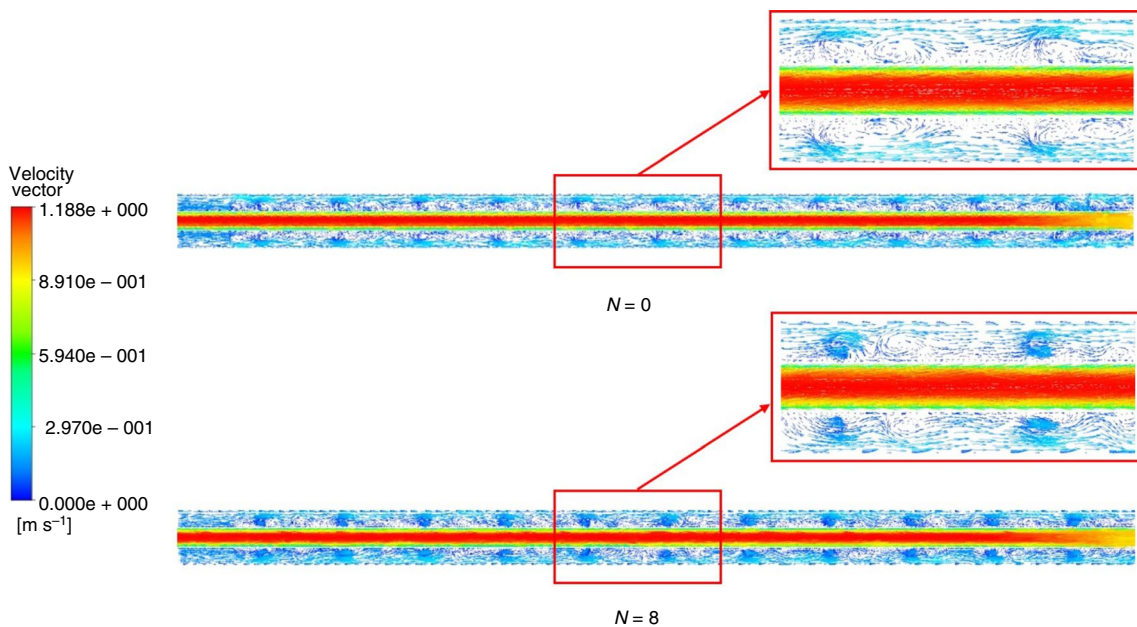
Fig. 10 Effect of number of holes N in the velocity vector field

with the Reynolds number, as it was observed with pure water in the previous subsections, the rotational speed increase has an additional effect of increasing the heat transfer coefficient, as shown in Fig. 11a, passing from around 7500 to 9500 W $(m^2 K)^{-1}$ for 500 rpm at the highest Reynolds numbers. This effect may be attributed to the increase in the swirling in the flow with rotation, which contributes to a better flow mixing and heat transfer to and from the tube walls.

Considering the effect of adding nanoparticles to the working fluid, when the nanoparticle concentration increases from 1 to 3%, all the curves shift upward, leading to higher heat transfer rates. When comparing the different nanofluids at the highest Reynolds number of 4946 and a concentration of 1%, the Cu-based nanofluid seems to perform better (35.46% improvement) than the hybrid Al_2O_3–Cu nanofluid (32.89%), with the Al_2O_3-based nanofluid achieving the smallest enhancement (25.62%), as shown in Fig. 11b–d. When the nanofluid concentration is increased to 2%, these percentages increase to 51.9%, 48.67%, and 43.75%, as shown in Fig. 11e–g. Finally, at 3% concentration, maximum enhancements of 54.23%, 53.19% and 50.34% are found for the Cu-based, the hybrid Al_2O_3–Cu, and the Al_2O_3-based nanofluids, respectively, as shown in Fig. 11h–j. The addition of nanoparticles to water increases fluid viscosity and thermal conductivity, resulting in a faster transfer of energy from the hotter temperature regions to the colder ones.

The values of the heat transfer coefficient obtained for water and the three nanofluids at 3% concentration are collected in Table 3, to allow for an exact comparison. The Cu–water nanofluid appears to be the one with the highest heat transfer enhancement, reaching values above 12,100 W $(m^2 K)^{-1}$ for a Reynolds number of 4946 when it is added at 3% concentration and the tube rotates at 500 rpm. The maximum limit of the hybrid Al_2O_3–Cu nanofluid is able to pass above 12,000 W $(m^2 K)^{-1}$ at the same conditions, whereas the Al_2O_3 nanofluid is only able to reach values slightly above 11,800 W $(m^2 K)^{-1}$. Therefore, in terms of enhancement of the heat transfer coefficient, the Cu-based nanofluid at 3% concentration is the preferable option.

Heat exchanger effectiveness

The effectiveness of the heat exchanger depending on the rotational speed and working fluid has been assessed as well. Figure 12 shows the results of adding Al_2O_3, Cu, and hybrid Al_2O_3–Cu nanoparticles to the working fluid from 1 to 3% concentration, combined with the effect of inner tube rotation up to 500 rpm in the range of Reynolds numbers from 2473 to 4946. As it happened with the heat transfer coefficient, the effectiveness increases as the Reynolds number, the rotational speed of the inner tube or the nanoparticle concentration increases. With pure water, it is possible to

increase the efficiency from around 27–39% when increasing the Reynolds number from 2473 to 4946, as shown in Fig. 12a. If this effect is combined with the rotation of the inner tube at 500 rpm, the efficiency can increase up to around 45%. Considering the different nanofluids, the Cu-based nanofluid exhibits again the best behavior, achieving efficiencies around 49%, 52% and 53% when it is added at 1, 2 and 3% concentration to the working fluid and the inner tube is rotated at 500 rpm. In second place, the hybrid Al_2O_3–Cu nanofluid reaches efficiencies of around 48%, 51% and 52%. Finally, the Al_2O_3-based nanofluid reaches efficiencies of around 46%, 50 and 51% when its concentration increases from 1 to 3%. Again, the most suitable nanofluid in terms of enhancing the effectiveness of the heat exchanger is the Cu-based nanofluid at 3% concentration, with a potential improvement of efficiency of 34.27% when the inner tube rotates at 500 rpm, compared with the 39% achieved without rotating the tube and using pure water.

Pressure drop

The pressure drop across the heat exchanger is a key parameter for dimensioning the required pumping power to drive the flow and must be considered if the energy consumption wants to be reduced, and an efficient heat exchanger design is sought.

With an initial pressure drop of around 40 Pa for pure water at the lowest Reynolds number of 2473 and without tube rotation, Fig. 13 shows the evolution of the pressure drop as the Reynolds number increases up to 4946, the tube rotational speed increases up to 500 rpm, and the three different nanofluids are added up to 3% concentration. Just by increasing the Reynolds number up to 4946 with pure water, the pressure drop increases up to around 120 Pa (300% increase). If, additionally, the inner tube of the exchanger is rotated, pressure drop values around 190 Pa are reached (475% increase). This may be explained by the increase in pressure drop that is produced by the increase in the fluid velocity linked to a higher Reynolds number. If the rotational speed is increased, it leads to an increase in tangential velocity, so the fluid must follow longer streamlines, having more space for reducing its pressure due to viscous effects. From these reference values, adding Al_2O_3 nanoparticles at 1, 2 and 3% concentrations can increase pressure drop up to around 195, 200 and 215 Pa. The hybrid Al_2O_3–Cu nanofluid reaches pressure drop values up to around 210, 215 and 230 Pa, whereas the Cu-based nanofluid presents the highest values, around 215, 225 and 235 Pa. The main reason behind the increase in the pressure drop is related to the increase in friction, due to the nanofluid viscosity, which ultimately depends on the nanoparticle concentration, but also on the changes in the thermal field. If only the pressure drop is to be considered in heat exchanger design, the addition of

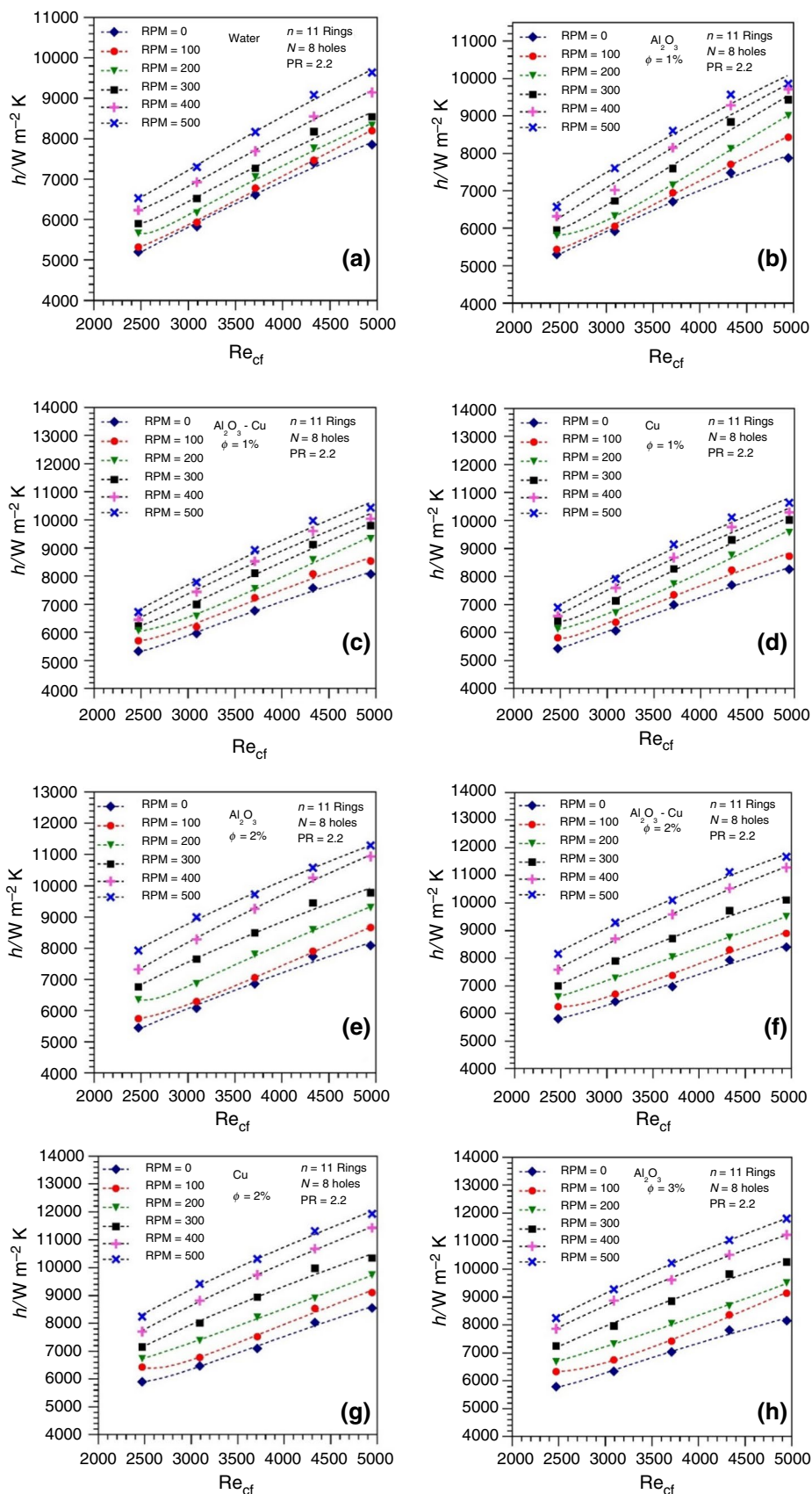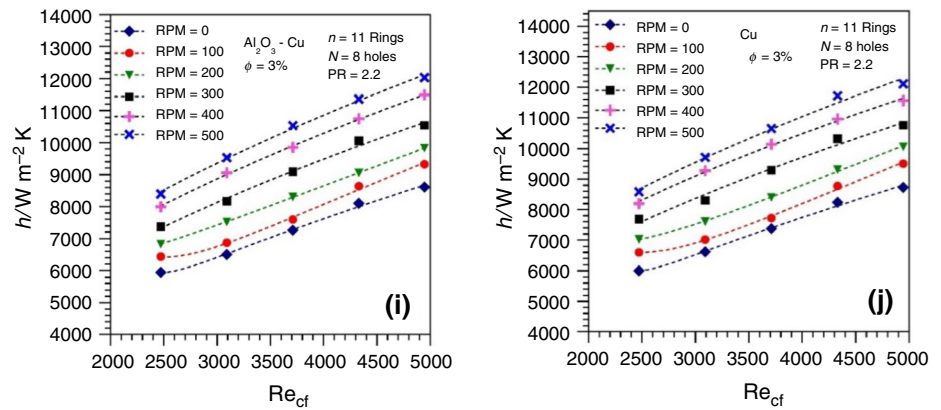**Fig. 11** Heat transfer coefficient as a function of rotational speed and concentration of nanofluid ϕ

Fig. 11 (continued)

Table 3 Heat transfer coefficient as a function of Reynolds number and rotational speed

Reynolds number	water			Cu-water at $\phi = 3\%$		
	h (0 RPM)	h (200 RPM)	h (500 RPM)	h (0 RPM)	h (200 RPM)	h (500 RPM)
2473	5200.20	5660.09	6526.94	5994.44	7021.76	8583.02
3092	5824.83	6164.85	7301.71	6613.15	7603.87	9707.23
3712	6615.08	7050.13	8169.19	7374.35	8399.45	10,656.76
4331	7402.99	7760.49	9083.27	8241.74	9317.45	11,724.93
4946	7852.76	8327.46	9638.61	8727.96	10,058.08	12,111.48
Reynolds number	Al$_2$O$_3$–Cu–water at $\phi = 3\%$			Al$_2$O$_3$–water at $\phi = 3\%$		
	h (0 RPM)	h (200 RPM)	h (500 RPM)	h (0 RPM)	h (200 RPM)	h (500 RPM)
2473	5947.2432	6830.1139	8394.8568	5795.3135	6684.3547	8252.948
3092	6504.1995	7523.223	9533.7494	6347.574	7319.9149	9278.1152
3712	7261.2332	8309.1901	10,536.854	7034.6592	8057.8769	10,217.84
4331	8102.5113	9054.9089	11,366.862	7825.3036	8682.066	11,040.619
4946	8613.4278	9833.4754	12,030.066	8156.4305	9507.7149	11,805.99

nanofluids seems detrimental to the design. Nevertheless, even in the worst scenario (Cu-based nanofluid at 3% and highest tube rotational speed of 500 rpm), a pressure drop of 235 Pa may be easily compensated by a low-cost pump. Considering the benefits regarding heat transfer enhancement of adding nanoparticles to the working fluid, it makes sense to continue choosing the Cu-based nanofluid at 3% concentration and try to compensate for the increase of around 200 Pa with pumping equipment.

Pumping power requirements

Due to the increase in the pressure drop, higher pumping power values will be required. The pumping power requirements for the different studied nanofluids as a function of concentration and rotational speed for the Reynolds number of 4946 are shown in Fig. 14. Looking at the results, it seems that the effect of the rotational speed increase is

more determining for the pumping power increase than the concentration of the nanofluid. This result aligns with the results obtained for the pressure drop in the previous subsection. Considering the cases without tube rotation at 1% concentration, around 94, 97 and 98 J kg^{-1} are required for the Al$_2$O$_3$, the Al$_2$O$_3$–Cu and the Cu nanofluids, respectively. When particle concentration increases to 3%, the increase in pumping power is just around 3 J kg^{-1} for all nanofluids. The increase in nanoparticles will increase fluid viscosity, but the effect of this increase in the pumping power is not so noticeable as the effect of increasing the rotational speed, which results in higher fluid velocities and extends the fluid streamlines, allowing for more friction. When the rotational speed is increased up to 500 rpm at 1% nanoparticle concentration, the increase in the pumping power required is around 21, 21.5 and 22 J kg^{-1} for the Al$_2$O$_3$, the Al$_2$O$_3$–Cu and the Cu nanofluids, respectively, seven times higher than the effect of increasing nanoparticle concentrations. If the tube

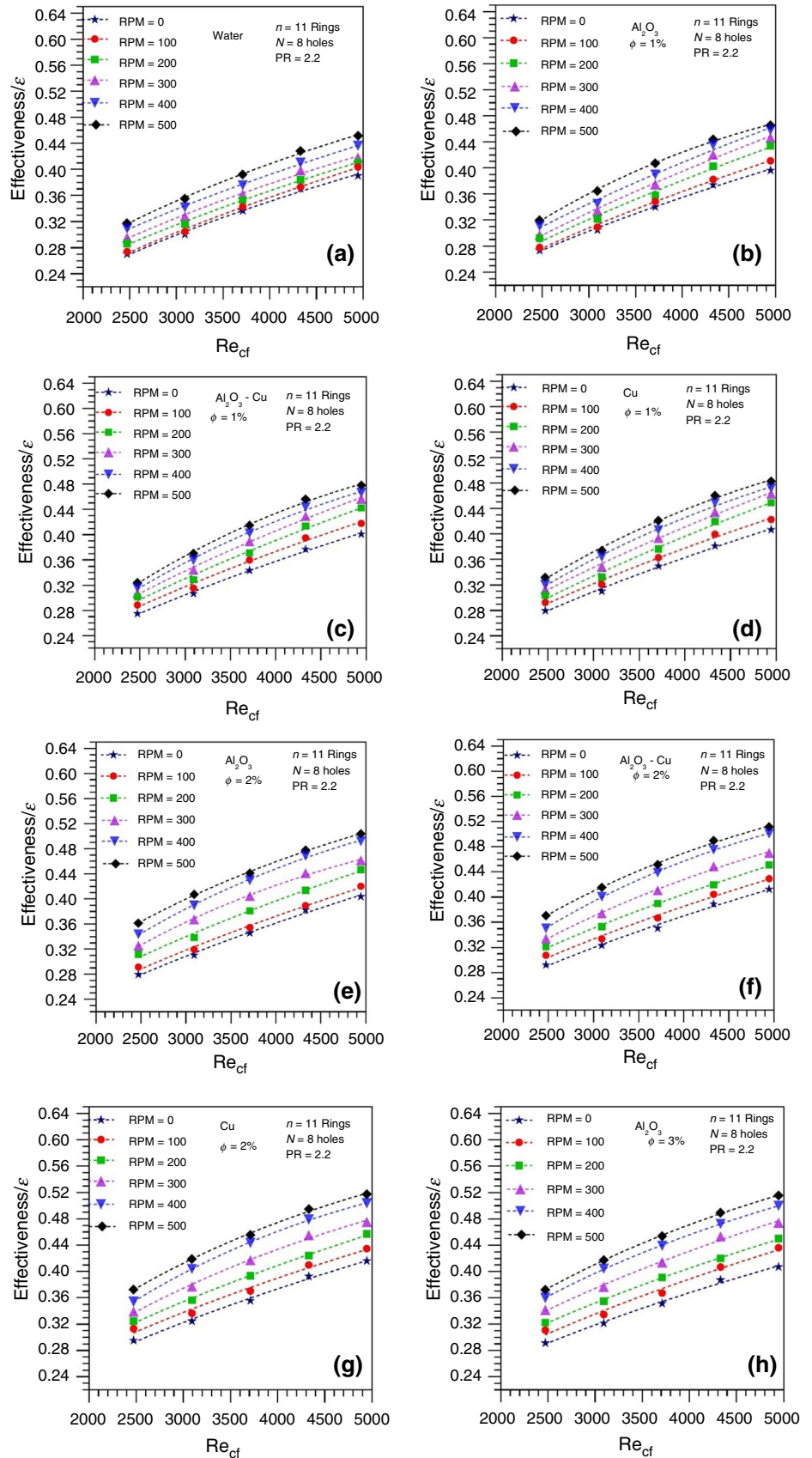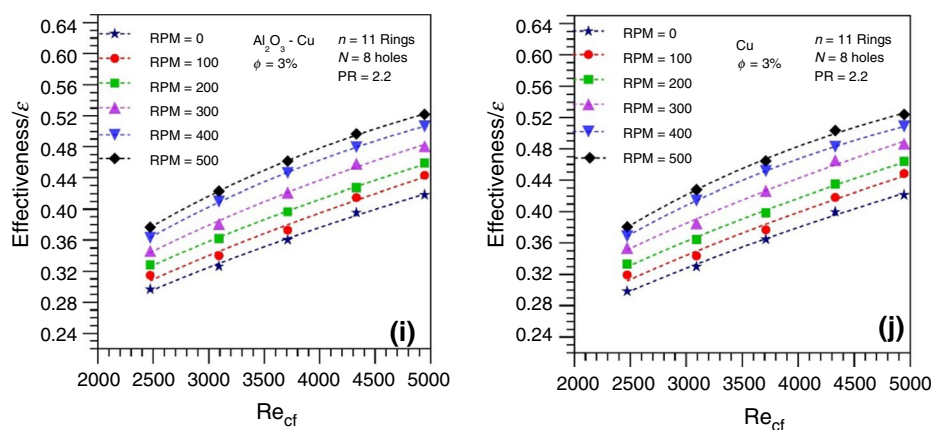**Fig. 12** Effectiveness as a function of rotational speed and concentration of nanofluid ϕ

Fig. 12 (continued)

rotates at 500 rpm and nanoparticles are added up to 3%, pumping power values required increase up to 117.5, 121 and 122.5 J kg^{-1} for the Al$_2$O$_3$, the Al$_2$O$_3$–Cu and the Cu nanofluids. Nevertheless, considering an average increase of around 0.01 kJ kg^{-1} in the pumping power requirements, only very high flowrate values through the exchanger would represent an actual problem. Therefore, it becomes justified to use the nanofluid with the best thermal behavior, the Cu–water based, at 3% concentration.

Description of flow and thermal fields

In order to provide a deeper description of the flow and thermal fields and provide insight into the underlying causes for the improvement of the heat exchanger efficiency with the selected configuration and operating characteristics, different variables describing them have been selected and will be commented in this subsection.

Figure 15 shows the turbulent kinetic energy contours along the longitudinal plane of the heat exchanger and near the ring zones. In the longitudinal plane, it may be appreciated how the rings are able to generate turbulence, increasing mixing and heat transfer accordingly and explaining why the introduction of rings improves heat transfer, with regions of high turbulence being convected downstream after each ring is placed. In the detail of the ring zones, it may be observed how each ring hole generates turbulent kinetic energy, which explains why heat transfer increases with the number of holes per ring. As the rotational speed of the inner tube is increased, the turbulence kinetic energy contours become more homogeneous, possibly as a consequence of the dispersion of this energy due to the rotational effects, hinting to a more efficient mixing of the flow and a more efficient heat convection.

With the aim of visualizing the flow, streamlines across the heat exchanger and at different cross sections are presented in Fig. 16 for the Reynolds numbers of 2473 and 4946 and 0, 200 and 500 rpm. There, the disturbance of

the predominantly axial flow caused by the perforated rings becomes apparent at 0 rpm, with vortex shedding phenomena that increase local momentum and heat transfer. After being convected downstream, dissipation of these vortices allows for the transfer of energy between the local vortex and the bulk flow. With the increase in the Reynolds number, the structures gain velocity, increasing convection accordingly. Nevertheless, these behaviors are associated with an increase in pressure drop, as it has been commented in the previous subsections. As the rotational speed increases up to 200, the flow structures start to become more diffuse, due to the smoothing effect of the rotational speed on. Nevertheless, two regions may be distinguished in each transversal plane: one corresponding to the region close to the rings and the inner tube, where a higher concentration of streamlines is found, and another one outside from this region up to the inner surface of the outer tube. This higher concentration of streamlines may explain the enhancement of heat transfer from the hot fluid toward the cold fluid region close to the inner tube, increasing the efficiency of the heat exchanger. Finally, at the rotational speed of 500 rpm, the shape of the streamlines changes from the axial behavior observed at 0 rpm to a helical shape. On the one hand, this means an increase in the effective path that each fluid particle follows inside the exchanger, allowing to exchange a higher amount of heat without increasing the real length of the exchanger tubes. On the other hand, the streamlines inside the region near the outer surface of the inner tube becomes highly intertwined, allowing the transfer of momentum and heat outside from the convective vortices shed by the rings more effectively.

Finally, temperature contours of the heat exchanger at cross sections located at different positions $z = 0.1$, 0.6 and 0.9 m are shown in Fig. 17 for the Reynolds numbers of 2473 and 4946 and 0, 200 and 500 rpm. It may be observed how the cold fluid increases its temperature when passing from $z = 0.1$ to 0.9, whereas the hot fluid decreases it when advancing from $z = 0.9$ to 0.1. The positive effect of

Fig. 13 Pressure drop as a function of rotational speed and concentration of nanofluid ϕ
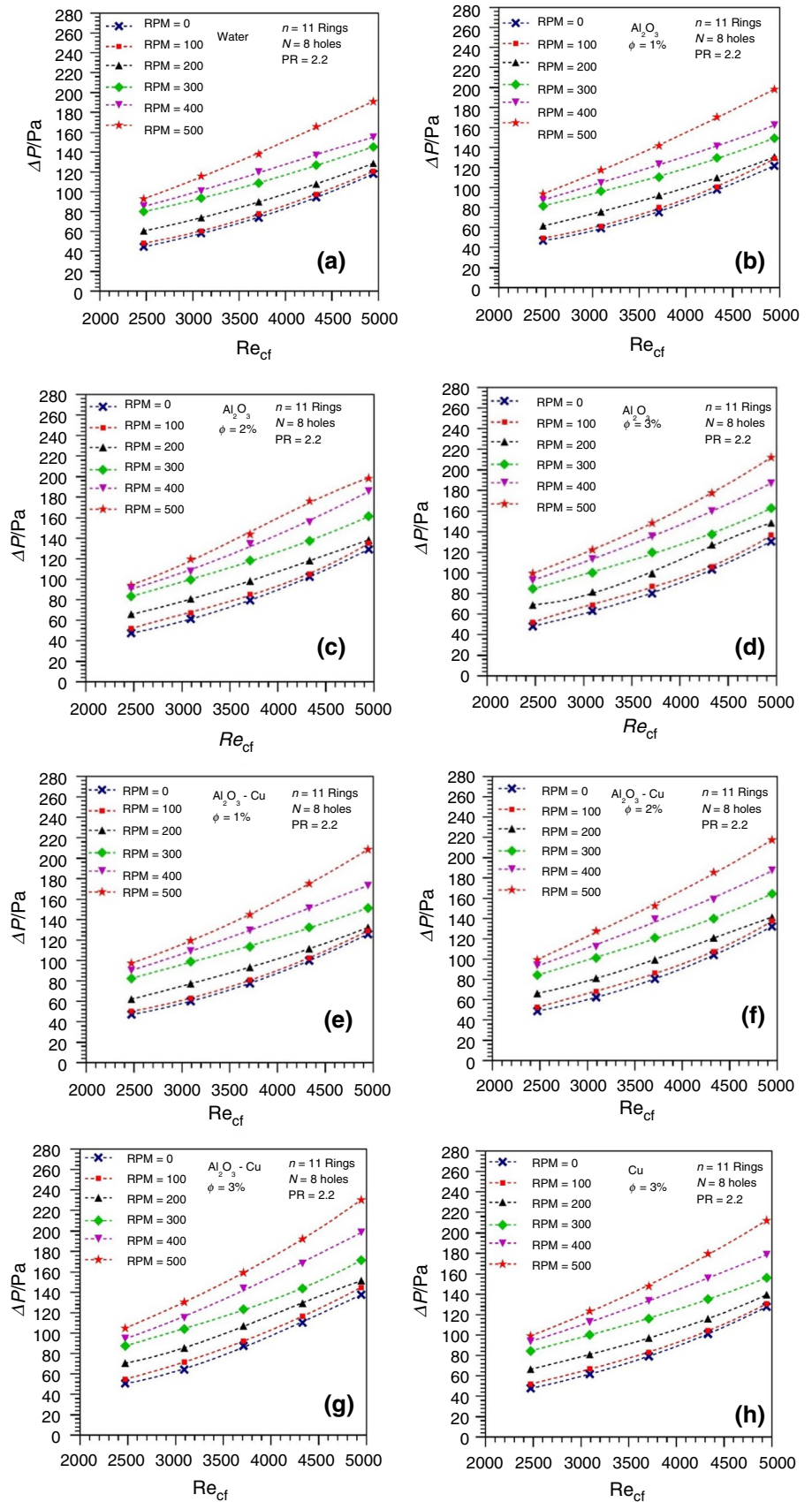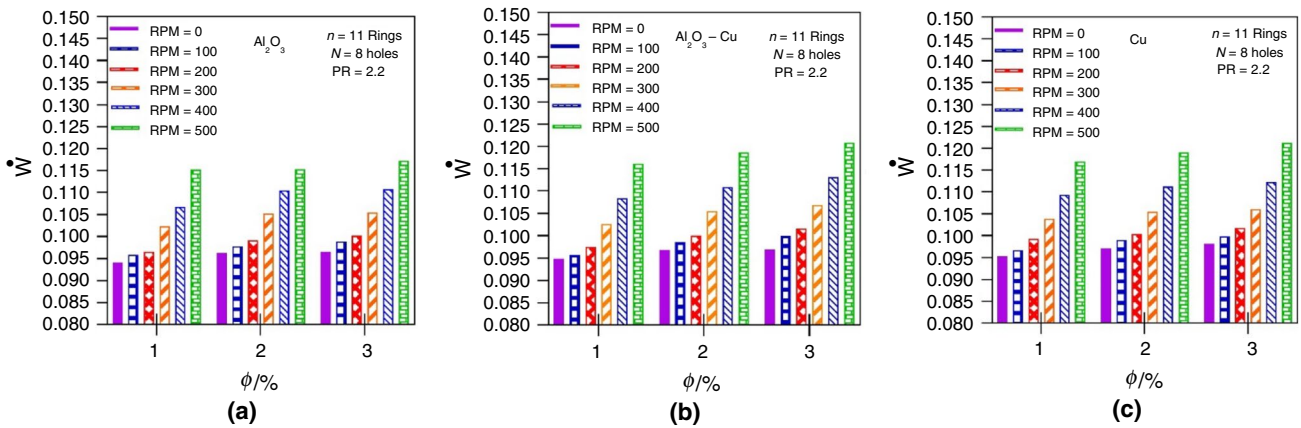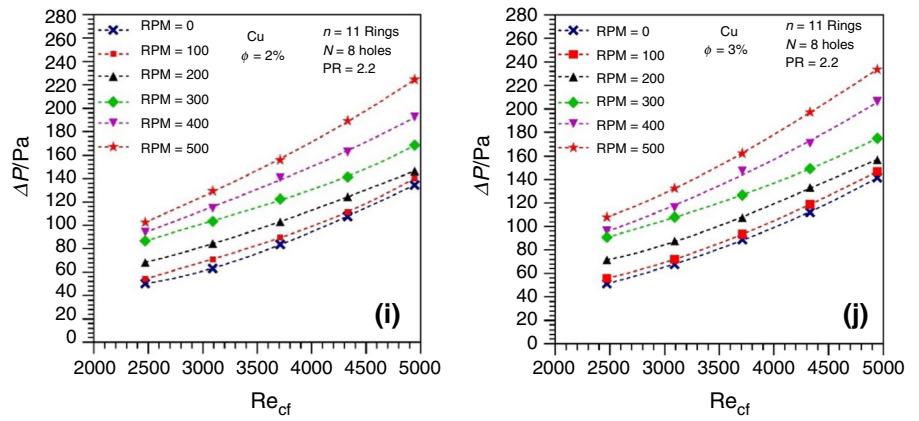
Fig. 13 (continued)

Fig. 14 Pumping power required as a function of rotational speed and concentration of nanofluid ϕ at $Re_{cf} = 4946$
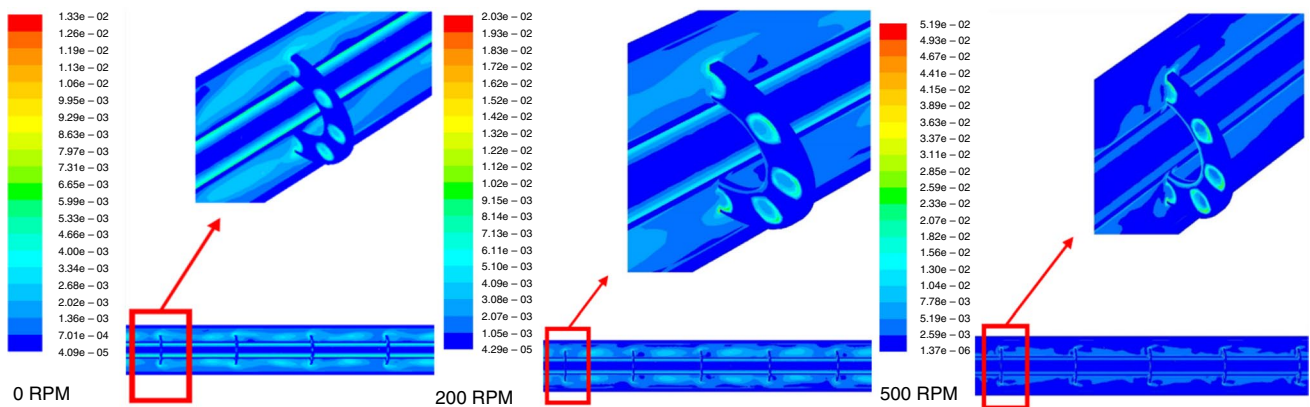

Fig. 15 Turbulence kinetic energy contours in longitudinal plane of the heat exchanger with detail of the rings

the rings on the thermal behavior of the heat exchanger becomes apparent, working as annular fins that increase the surface area in contact with the fluid and help transport thermal energy from the hot fluid to the cold one. The effect of the ring holes is also visible, leading to the "gear"-like

patterns observed at $z = 0.1$ and $z = 0.6$, indicating modifications of the temperature gradients consequent with a better heat transfer. Finally, it may be observed how, with the increase in the rotational speed, all patterns become more

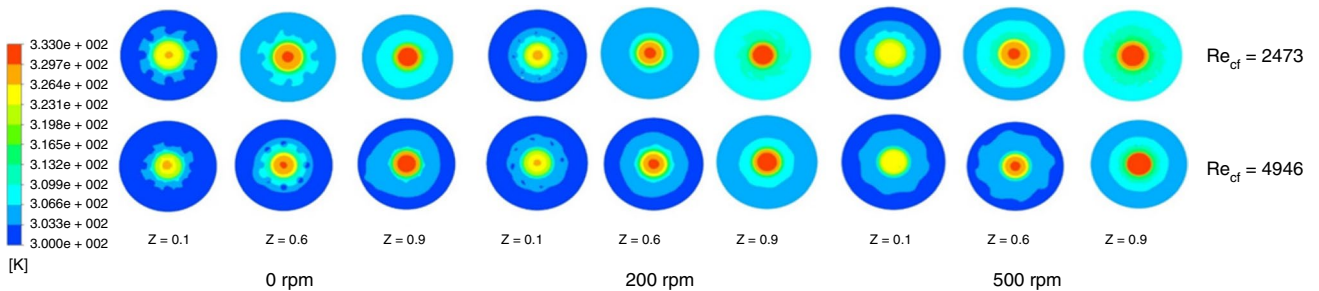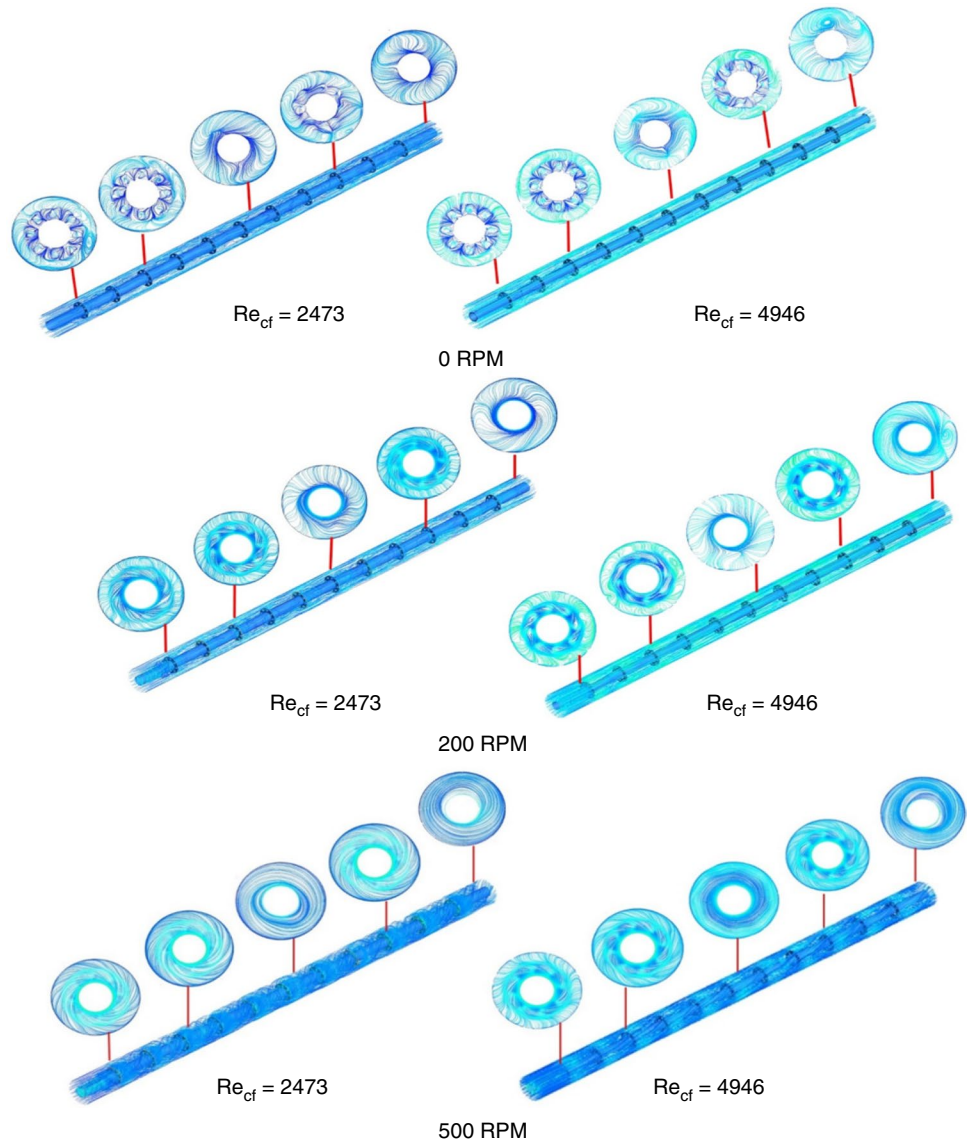**Fig. 16** Streamlines across the heat exchanger and at different sections

Fig. 17 Temperature contours at different cross sections of the heat exchanger

homogeneous, thanks to a faster heat transfer caused by the swirling flow.

Conclusions

In the present work, the performance of a tube heat exchanger combining the effects of a rotating tube and perforated ring inserts when Al_2O_3, Cu and hybrid Al_2O_3–Cu nanofluids are used as working fluids has been studied. This has allowed to increase the heat transfer efficiency for a given heat exchanger size, potentially reducing heat exchanger sizes for a given heat power to be transferred.

After developing a three-dimensional numerical model of the exchanger, verifying the numerical discretization and validating the results of the model with experiments, optimization of the geometrical parameters was sought, using the heat transfer coefficient and pressure drop as optimization variables. It was concluded that the best heat exchanger configuration included 11 rings with eight holes per ring placed on the inner tube outer surface with a pitch ratio of 2.2, allowing to increase the heat transfer coefficient due to turbulence generation and mixing. At the same time, the pressure drop increase was kept relatively low thanks to the presence of holes that reduced flow resistance.

Once the geometrical configuration of the heat exchanger was optimized, it was found that the heat transfer coefficient improved substantially when increasing the Reynolds number of the cold fluid up to 4946, and the rotational speed up to 500 rpm, achieving an increase from around 7500 to 9500 W $(m^2\ K)^{-1}$. Considering the different nanofluids studied, the Cu nanofluid showed the best performance, the Al_2O_3–Cu hybrid fluid presented intermediate values, and the Al_2O_3 nanofluid exhibiting the lowest improvements with respect to pure water. When nanoparticles of Cu, the ones with the best behavior, were added to the working fluid at 3% concentration, the coefficient increased above 12,100 W $(m^2\ K)^{-1}$. Regarding the effectiveness of the heat exchanger, it is equivalent to passing from 27 to 51%. On the other hand, these actions increase the pressure drop of the exchanger from the original 40 Pa for water and without rotating the inner tube to 235 Pa. Nevertheless, 0.2 kPa may be easily compensated by a low-cost pump. The increase in the pumping requirements for this situation are around 0.1 kJ kg^{-1}, so only very high flowrate values through the exchanger would represent an actual problem. Therefore, it becomes justified to use the nanofluid with the best thermal behavior, the Cu-based, at 3% concentration.

Explanations for the underlying physical phenomena that cause the increase in heat transfer due to the rotational speed of the inner tube, the addition of perforated rings and the use of nanofluids were provided. Turbulent kinetic energy

contours, flow streamlines, and temperature contours were used to gain insight into the thermal and flow fields, identifying the mechanisms responsible for the enhancement of the heat exchanger effectiveness.

Many engineering applications, such as waste heat recovery processes, air-conditioning and refrigeration systems, may be benefited from implementing the geometry proposed in this study and combining the use of nanofluids with the rotation of the heat exchanger tubes.

Declarations

References

1. Watel B, Harmand S, Desmet B. Infuence of fin spacing and rotational speed on the convective heat exchanges from a rotating finned tube. Int J Heat Fluid Flow. 2000;21:221–7.
2. Yakut K, Sahin B. Flow-induced vibration analysis of conical rings used for heat transfer enhancement in heat exchangers. Appl Energy. 2004;78:273–88.
3. Chen HT, Hsu WL. Estimation of heat transfer coefficient on the fin of annular-finned tube heat exchangers in natural convection for various fin spacings. Int J Heat Mass Transf. 2007;50:1750–61.
4. Kongkaitpaiboon V, Nanan K, Eiamsa-ard S. Experimental investigation of convective heat transfer and pressure loss in a round tube fitted with circular-ring turbulators. Int Commun Heat Mass Transf. 2010;37:568–74.
5. Duangthongsuk W, Wongwises S. An experimental study on the heat transfer performance and pressure drop of TiO2-water nanofluids flowing under a turbulent flow regime. Int J Heat Mass Transf. 2010;53:334–44.
6. Yang C, Li W, Nakayama A. Convective heat transfer of nanofluids in a concentric annulus. Int J Therm Sci. 2013;71:249–57.
7. Darzi AAR, Farhadi M, Sedighi K, Aallahyari S, Delavar MA. Turbulent heat transfer of Al_2O_3–water nanofluid inside helically corrugated tubes: numerical study. Int Commun Heat Mass Transf. 2013;41:68–75.
8. Madhesh D, Parameshwaran R, Kalaiselvam S. Experimental investigation on convective heat transfer and rheological characteristics of Cu–TiO_2 hybrid nanofluids. Exp Thermal Fluid Sci. 2014;52:104–15.

9. Ard SE, Kiatkittipong K. Heat transfer enhancement by multiple twisted tape inserts and TiO$_2$/water nanofluid. Appl Therm Eng. 2014;70:896–924.

10. Reddy MCS, Rao VV. Experimental investigation of heat transfer coefficient and friction factor of ethylene glycol water based TiO$_2$ nanofluid in double pipe heat exchanger with and without helical coil inserts. Int Commun Heat Mass Transf. 2014;50:68–76.

11. Chokphoemphun S, Pimsarn M, Thianpong C, Promvonge P. Heat transfer augmentation in a circular tube with winglet vortex generators. Chin J Chem Eng. 2015;23:605–14.

12. Huang WC, Chen CA, Shen C, San JY. Effects of characteristic parameters on heat transfer enhancement of repeated ring-type ribs in circular tubes. Exp Thermal Fluid Sci. 2015;68:371–80.

13. Singh V, Chamoli S, Kumar M, Kumar A. Heat transfer and fluid flow characteristics of heat exchanger tube with multiple twisted tapes and solid rings inserts. Chem Eng Process. 2016;102:156–68.

14. Sheikholeslami M, Bandpy MG, Ganji DD. Experimental study on turbulent flow and heat transfer in an air to water heat exchanger using perforated circular-ring. Exp Thermal Fluid Sci. 2016;70:185–95.

15. Sheikholeslami M, Ganji DD, Bandpy MG. Experimental and numerical analysis for effects of using conical ring on turbulent flow and heat transfer in a double pipe air to water heat exchanger. Appl Therm Eng. 2016;100:805–19.

16. Sripattanapipat S, Tamna S, Jayranaiwachira N, Promvonge P. Numerical heat transfer investigation in a heat exchanger tube with hexagonal conical-ring inserts. Energy Procedia. 2016;100:522–5.

17. Hazbehian M, Maddah H, Mohammadiun H, Alizadeh M. Experimental investigation of heat transfer augmentation inside double pipe heat exchanger equipped with reduced width twisted tapes nserts using polymeric nanofluid. Heat Mass Transf. 2016;52:2515–29.

18. Bajestan EE, Moghadam MC, Niazmand H, Daungthongsuk W, Wongwises S. Experimental and numerical investigation of nanofluids heat transfer characteristics for application in solar heat exchangers. Int J Heat Mass Transf. 2016;92:1041–52.

19. Saeedan M, Nazar ARS, Abbasi Y, Karimi R. CFD Investigation and neutral network modeling of heat transfer and pressure drop of nanofluids in double pipe helically baffled heat exchanger with a 3D fined tube. Appl Therm Eng. 2016;100:721–9.

20. El-Maghlany WM, Hanafy AA, Hassan AA, El-Magid MA. Experimental study of Cu–water nanofluid heat transfer and pressure drop in a horizontal double-tube heat exchanger. Exp Thermal Fluid Sci. 2016;78:100–11.

21. Abou-Ziyan HZ, Helali AHB, Selim MYE. Enhancement of forced convection in wide cylindrical annular channel using rotating inner pipe with interrupted helical fins. Int J Heat Mass Transf. 2016;95:996–1007.

22. Gomaa A, Halim MA, Elsaid AM. Experimental and numerical investigations of a triple concentric-tube heat exchanger. Appl Therm Eng. 2016;99:1303–15.

23. Forooghi P, Flory M, Bertsche D, Wetzel T, Frohnapfel B. Heat transfer enhancement on the liquid side of an industrially designed flat-tube heat exchanger with passive inserts—numerical investigation. Appl Therm Eng. 2017;123:573–83.

24. Rao MSE, Sreeramulu D, Rao CJ, Ramana MV. Experimental investigation on forced convective heat transfer coefficient of a nano fluid. Mater Today Proc. 2017;4:8717–23.

25. Kumar NTR, Bhramara P, Addis BM, Sundar LS, Singh MK, Sousa ACM. Heat transfer, friction factor and effectiveness analysis of Fe$_3$O$_4$/water nanofluid flow in a double pipe heat exchanger with return bend. Int Commun Heat Mass Transf. 2017;81:155–63.

26. Babu JAR, Kumar KK, Rao SS. State-of-art review on hybrid nanofluids. Renew Sustain Energy Rev. 2017;77:551–65.

27. Liang G, Islam MD, Kharoua N, Simmons R. Numerical study of heat transfer and flow behavior in a circular tube fitted with varying arrays of winglet vortex generators. Int J Therm Sci. 2018;134:54–65.

28. Skullong S, Promvonge P, Thianpong C, Jayranaiwachira N, Pimsarn M. Thermal performance of heat exchanger tube inserted with curved winglet tapes. Appl Therm Eng. 2018;129:1197–211.

29. Liu P, Zheng N, Shan F, Liu Z, Liu W. An experimental and numerical study on the laminar heat transfer and flow characteristics of a circular tube fitted with multiple conical strips inserts. Int J Heat Mass Transf. 2018;117:691–709.

30. Bartwala A, Gautamb A, Kumara M, Mangrulkarc CK, Chamolia S. Thermal performance intensification of a circular heat exchanger tube integrated with compound circular ring–metal wire net inserts. Chem Eng Process. 2018;124:50–70.

31. Ali MAM, El-Maghlany WM, Eldrainy YA, Attia A. Heat transfer enhancement of double pipe heat exchanger using rotating of variable eccentricity inner pipe. Alex Eng J. 2018;57:3709–25.

32. Siadaty M, Kazazi M. Study of water based nanofluid flows in annular tubes using numerical simulation and sensitivity analysis. Heat Mass Transf. 2018;54:2995–3014.

33. Muszynski T, Andrzejczyk R. Experimental study on single phase operation of microjet augmented heat exchanger with enhanced heat transfer surface. Appl Therm Eng. 2019;155:289–96.

34. Al-Obaidi AR. Investigation of fluid field analysis, characteristics of pressure drop and improvement of heat transfer in three-dimensional circular corrugated pipes. J Energy Storage. 2019;26:101012.

35. Nakhchi ME, Esfahani JA. Numerical investigation of turbulent Cu–water nanofluid in heat exchanger tube equipped with perforated conical rings. Adv Powder Technol. 2019;30:1338–47.

36. Nakhchi ME, Esfahani JA. Numerical investigation of different geometrical parameters of perforated conical rings on flow structure and heat transfer in heat exchangers. Appl Therm Eng. 2019;156:494–505.

37. Ibrahim MM, Essa MA, Mostafa NH. A computational study of heat transfer analysis for a circular tube with conical ring turbulators. Int J Therm Sci. 2019;137:138–60.

38. Mohammed HA, Abuobeida IAMA, Vuthalurua HB, Liu S. Two-phase forced convection of nanofluids flow in circular tubes using convergent and divergent conical rings inserts. Int Commun Heat Mass Transf. 2019;101:10–20.

39. Nada SA, Said MA. Effects of fins geometries, arrangements, dimensions and numbers on natural convection heat transfer characteristics in finned-horizontal annulus. Int J Therm Sci. 2019;137:121–37.

40. Yadav S, Sahu SK. Heat transfer augmentation in double pipe water to air counter flow heat exchanger with helical surface disc turbulators. Chem Eng Process. 2019;135:120–32.

41. Qi C, Luo T, Liu M, Fan F, Yan Y. Experimental study on the flow and heat transfer characteristics of nanofluids in double-tube heat exchangers based on thermal efficiency assessment. Energy Convers Manag. 2019;197:111877.

42. Bahiraeia M, Mazaherib N, Mohammadmic MS, Moayedi H. Thermal performance of a new nanofluid containing biologically functionalized graphene nanoplatelets inside tubes equipped with rotating coaxial double-twisted tapes. Int Commun Heat Mass Transf. 2019;108:104305.

43. Bezaatpour M, Goharkhah M. Convective heat transfer enhancement in a double pipe mini heat exchanger by magnetic field induced swirling flow. Appl Therm Eng. 2020;167:114801.

44. Thejaraju R, Girisha KB, Manjunath SH, Dayananda BS. Experimental investigation of turbulent flow behavior in an air to air double pipe heat exchanger using novel para winglet tape. Case Stud Therm Eng. 2020;22:100791.

45. Bahiraei M, Mazaheri N, Hosseini S. Neural network modeling of thermo-hydraulic attributes and entropy generation of an eco-friendly nanofluid flow inside tubes equipped with novel rotary coaxial double-twisted tape. Powder Technol. 2020;369:162–75.

46. Murali G, Nagendra B, Jaya J. CFD analysis on heat transfer and pressure drop characteristics of turbulent flow in a tube fitted with trapezoidal-cut twisted tape insert using Fe_3O_4 nanofluid. Mater Today Proc. 2020;21:313–9.

47. Singh SK, Sarkar J. Improving hydrothermal performance of hybrid nanofluid in double tube heat exchanger using tapered wire coil turbulator. Adv Powder Technol. 2020;31:2092–100.

48. Jasim LM, Hamzah H, Canpolat C, Sahin B. Mixed convection flow of hybrid nanofluid through a vented enclosure with an inner rotating cylinder. Int Commun Heat Mass Transf. 2021;121:105086.

49. Moayedi H. Investigation of heat transfer enhancement of Cu–water nanofluid by different configurations of double rotating cylinders in a vented cavity with different inlet and outlet ports. Int Commun Heat Mass Transf. 2021;126:105432.

50. Singh DK, Ahmad W, Kumar R. Two phase nanofluid flow and heat transfer characteristics in smooth horizontal tube installed by twisted tapes with alternate axes of rotation. J Braz Soc Mech Sci Eng. 2021;43:553.

51. Fathi MI, Mussa MA. Experimental study on the effect of tube rotation on performance of horizontal shell and tube latent heat energy storage. J Energy Storage. 2021;39:102626.

52. Heydari A, Goharimanesh M, Gharib MR. Dynamic viscosity analysis of hybrid nanofluid MWCNT-Al_2O_3/engine oil using statistical models with evaluating its performance in a double tube heat exchanger. J Therm Anal Calorim. 2023;148:8025–39.

53. Pali HS, Sharma A, Kumar M, Annakodi VA, Nguyen VN, Singh NK, Balasubramanian D, Deepanraj B, Truong TH, Nguyen PQP. Enhancement of combustion characteristics of waste cooking oil biodiesel using TiO_2 nanofluid blends through RSM. Fuel. 2023;331:125681.

54. Murugesan P, Elumalai PV, Balasubramanian D, Padmanabhan S, Murugunachippan N, Afzal A, Sharma P, Kiran K, Josephin JF, Varuvel EG, Le TT. Exploration of low heat rejection engine characteristics powered with carbon nanotubes-added waste plastic pyrolysis oil. Process Saf Environ Prot. 2023;176:1101–19.

55. Krupakaran RL, Gangula VR, Tarigonda H, Sachuthananthan B, Balasubramanian D, Anchupogu P, Petla R, Veerasamy S. The influence of thermal barrier coating (TBC) on diesel engine performance powered by using Mimusops elengi methyl ester with TiO_2 nanoadditive. Int J Ambient Energy. 2023;44:2250–61.